DNA Translocation Governed by Interactions with Solid-State Nanopores

Meni Wanunu, Jason Sutin, Ben McNally, Andrew Chow, and Amit Meller
Department of Biomedical Engineering and Department of Physics, Boston University, Boston, Massachusetts

ABSTRACT We investigate the voltage-driven translocation dynamics of individual DNA molecules through solid-state nanopores in the diameter range 2.7–5 nm. Our studies reveal an order of magnitude increase in the translocation times when the pore diameter is decreased from 5 to 2.7 nm, and steep temperature dependence, nearly threefold larger than would be expected if the dynamics were governed by viscous drag. As previously predicted for an interaction-dominated translocation process, we observe exponential voltage dependence on translocation times. Mean translocation times scale with DNA length by two power laws: for short DNA molecules, in the range 150–3500 bp, we find an exponent of 1.40, whereas for longer molecules, an exponent of 2.28 dominates. Surprisingly, we find a transition in the fraction of ion current blocked by DNA, from a length-independent regime for short DNA molecules to a regime where the longer the DNA, the more current is blocked. Temperature dependence studies reveal that for increasing DNA lengths, additional interactions are responsible for the slower DNA dynamics. Our results can be rationalized by considering DNA/pore interactions as the predominant factor determining DNA translocation dynamics in small pores. These interactions markedly slow down the translocation rate, enabling higher temporal resolution than observed with larger pores. These findings shed light on the transport properties of DNA in small pores, relevant for future nanopore applications, such as DNA sequencing and genotyping.

INTRODUCTION

Nanopores are an emerging class of single-molecule sensors capable of probing the properties of nucleic acids and proteins with high-throughput and resolution (1–3). In a nanopore experiment, voltage is applied across a thin insulating membrane containing a nanoscale pore, and the ion current of an electrolyte flowing through the pore is measured. Upon introduction of charged biopolymers to the solution, the local electrical field drives individual molecules through the nanopore. Passage of biopolymers through the pore causes distinct ion current signals, with amplitudes that directly correspond to their properties. Among single-molecule sensors, nanopores are unique because molecules can be probed without chemical modification and/or surface immobilization, thus preserving structure/function and allowing very high throughput. These attractive features have set the stage for the development of novel nanopore-based applications, such as detection of genetic variability, probing DNA-protein interactions, and low-cost, high-throughput DNA sequencing (4–6).

Central to all nanopore methods is the need for control over the translocation process at a level that allows spatial information to be resolved at the nanometer scale, within the finite time resolution imposed by instrumental bandwidth. Ultimately, fundamental understanding of the factors governing the DNA translocation dynamics, and its relationship with the magnitude and fluctuations of the blocked current signal, is necessary to achieve this goal. To date, most DNA translocation studies have been performed using the toxin α-hemolysin (α-HL), which can only admit single-stranded (ss) nucleic acids (7–9). The linear dependence of the most probable translocation time (t_P) on ssDNA length (l), and the lack of strong sticking interactions between the nucleic acids and α-HL, have supported the idea that the translocation process can be approximated by a mean sliding velocity $\langle v_T \rangle \sim 0.2$ nm/μs (measured for ssDNA at 120 mV and room temperature), or an average translocation rate $t_P = l/N\langle v_T \rangle \approx 2$ μs/base (where N is the number of nucleotides). This rate provides sufficient temporal resolution for detecting a few bases within instrumental bandwidth limits (9,10). However, prospective biotechnological nanopore applications require size tunability and membrane robustness, not available with phospholipid-embedded protein channels.

Recent progress in the fabrication of nanoscale materials has enabled the reproducible formation of artificial, well-defined nanopores in thin, solid-state membranes (11–13). Most DNA translocation studies have focused on relatively large pores (8–20 nm), for which average translocation dynamics were markedly faster than those reported for α-HL ($\langle v_T \rangle \sim 10$ nm/μs, or 30 ns/bp) (14–18). Broad dwell-time distributions for DNA translocation have been previously reported with smaller solid-state nanopores (2–3 nm) (14,19), although the source of broadening and the nature of the dwell-time events were not investigated experimentally. To slow the translocation dynamics, several experimental parameters have been modified, including viscosity, temperature, and voltage. However, these parameters also reduce the open-pore current, thereby degrading the blocked current signal (20). Moreover, an increase in the bulk viscosity or a reduction of the driving voltage reduces DNA diffusion to the pore and

Submitted June 19, 2008, and accepted for publication August 13, 2008.

Address reprint requests to Amit Meller, Dept. of Biomedical Engineering, Boston University, Boston, MA 02215. E-mail: ameller@bu.edu.

Editor: Taekjip Ha.

0006-3495/08/11/4716/10 $2.00

doi: 10.1529/biophysj.108.140475

the capture probability, respectively, therefore decreasing the overall throughput (21).

In this article, we focus on the use of nanopore/DNA interactions as an alternative means to slow down DNA translocation through nanopores, by using nanopores only slightly larger than a double-stranded DNA (dsDNA) cross section. Theoretically, interactions have been proposed to dominate the dynamics for both α-HL (22) and synthetic (19,23,24) nanopores, in particular for nanopore dimensions slightly larger than the molecular cross section (2.2 nm for dsDNA).

DNA analysis using nanopores via single-file threading (i.e., by unfolded entry) is highly attractive, potentially allowing detection of subtle variations in local DNA structure as it transverses the pore, for example, single- and double-stranded regions on a DNA template. To promote unfolded DNA entry while simultaneously maximizing DNA/surface interactions, we have focused in this study on solid-state nanopores in the range 2.7–5 nm. Our results show that small variations in the nanopore diameter strongly affect average translocation times, the threading probability, and the event current amplitude. Also, translocation times exhibit steep temperature dependence, nearly three times larger than expected from viscosity changes. Our results clearly show that DNA/pore interactions are the dominant contributing factor governing DNA translocation through small pores, revealing a more complex DNA translocation dynamics than previously observed.

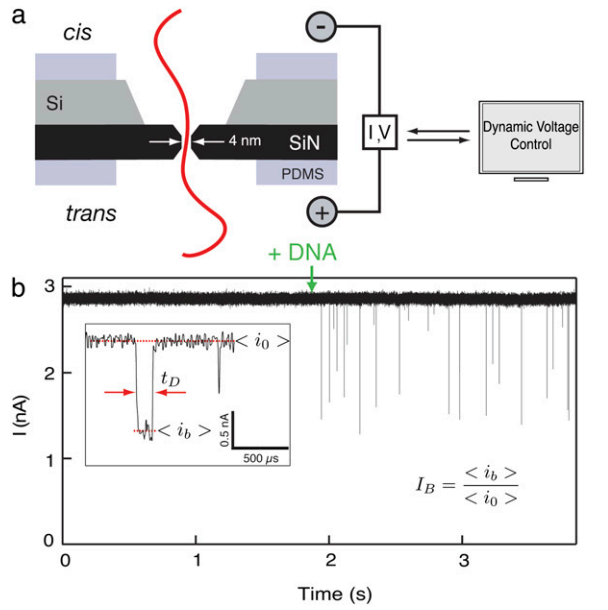

FIGURE 1 (*a*) Schematic illustration of a solid-state nanopore device for probing DNA translocation dynamics (not to scale). DNA molecules are driven through the nanopore by an applied voltage while the ion current of an electrolyte is measured. Dynamic voltage control is used to automatically unclog the pore when a molecule remains in the pore for >5 s. Hourglass-shaped nanopores with diameters in the range $3 < d < 8$ nm and effective thickness of ~10 nm were used (see text). (*b*) A typical ion-current trace for a 4-nm pore, before and after the introduction of 5 nM 400-bp DNA to the *cis* chamber (*green arrow*). The transient current-blockade events correspond to single-molecule translocation of DNA. The inset displays a magnified translocation event, in which the relevant parameters used in this article are defined.

MATERIALS AND METHODS

Nanopores were fabricated in 25- to 30-nm-thick, low-stress SiN windows (25 μm × 25 μm) supported by a Si chip (Protochips, Raleigh, NC), using a focused electron beam (13). Extensive transmission electron microscopic tomography studies revealed an hourglass nanopore profile with an effective thickness of ~⅓ the membrane thickness (~10 nm for the 30-nm membrane in this study). Nanopore chips were cleaned and assembled on a custom-designed cell under controlled atmosphere (see Wanunu and Meller (3) for details). After the addition of degassed and filtered 1 M KCl electrolyte (buffered with 10 mM Tris-HCl to pH 8.5), the nanopore cell was placed in a custom-designed chamber featuring thermoelectric regulation within ±0.1°C, rapid thermal equilibration (<5 min), and an effective electromagnetic shield. Ag/AgCl electrodes were immersed into each chamber of the cell and connected to an Axon 200B headstage. All measurements were taken inside a dark Faraday cage. DNA was introduced to the *cis* chamber, and a positive voltage of 300 mV was applied to the *trans* chamber in all experiments.

For the DNA length dependence studies we used a series of pure, linear DNA fragments with lengths in the range 150–20,000 bp (NoLimits, Fermentas, Burlington, Ontario, Canada). Agarose gel electrophoresis confirmed the purity of each DNA sample (see the Supplementary Material, Fig. S1 in Data S1). All DNA samples were heated to 70°C for 10 min before use. Our solid-state nanopore setup is displayed schematically in Fig. 1 *a*. Upon addition of dsDNA into the *cis* chamber (Fig. 1 *b*, *green arrow*), we observe distinct, stochastic current blockade events, the rates of which scale with DNA concentration. A trace of current blockade events with an expanded time axis is shown in the inset to Fig. 1 *b*. Several parameters are defined here: the event duration (or dwell-time), t_D, the mean blocked-pore current, $\langle i_b \rangle$, and the dimensionless fractional current, $I_B = \langle i_b \rangle / \langle i_o \rangle$, where $\langle i_o \rangle$ is the open-pore current. $1 - I_B$ is the event amplitude (e.g., $1 - I_B = 0$ when the pore is fully open, and thus, $\langle i_b \rangle = \langle i_o \rangle$; in a similar way, a fully blocked pore corresponds to $1 - I_B = 1$ or $\langle i_b \rangle = 0$). The use of normalized units facilitates the comparison of event amplitudes between measurements using different pore sizes or other conditions that alter the open-pore current (e.g., temperature). All measurements reported in this article were performed using a 75 kHz low-pass filter, and sampled using a 16-bit/250 KHz DAQ card. Under these conditions, the maximum error in $\langle i_b \rangle$ determination for the shortest dwell-times we can measure (12 μs) is <3%, as determined experimentally (Fig. S2, Data S1).

Continuous-time recordings of a 4-nm pore at 300 mV (1 M KCl, 21°C, pH 8.5) for different concentrations of 400-bp DNA in the *cis* chamber are shown in Fig. 2 *a*. As expected from this stochastic process, we find that delay times between successive events (δt) follow monoexponential distributions (25), with timescales corresponding to average event rates. For the same DNA fragment, the event rate grows linearly with DNA concentration, as shown in Fig. 2 *b*. PCR experiments were performed to verify that DNA molecules cross the membrane (from *cis* to *trans*) only upon application of positive voltage to the *trans* chamber (Fig. S3, Data S1).

RESULTS

We first describe our data and the methods used to analyze blocked-current and dwell-time distributions, and then discuss the effect of pore size on the DNA capture probability, the translocation dynamics, and the blocked current. The last Results section is focused on dependence of the translocation dynamics on DNA length, temperature, and voltage. See Table 1 for a glossary of symbols.

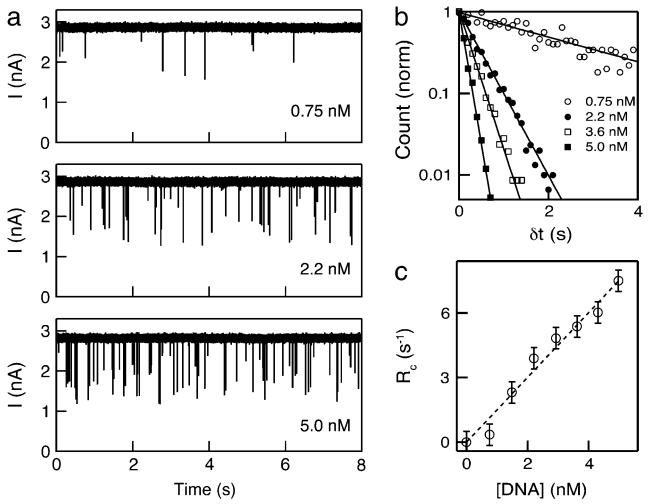

FIGURE 2 Translocation recordings for a 400-bp DNA fragment using a 4-nm pore at 1 M KCl, pH 8.5, 300 mV. (*a*) Continuous current recordings showing blockade events at the indicated DNA concentrations. (*b*) Normalized distributions of time delay between successive events for different concentrations, using the same pore and DNA as in *a*, with monoexponential fits to the distributions. (*c*) A plot of the average event rate as a function of DNA concentration, showing a linear dependence.

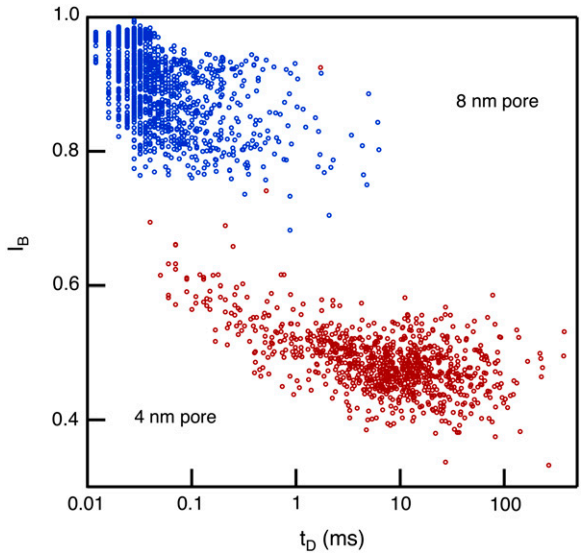

FIGURE 3 Semilog I_B versus t_D scatter plots measured for 8000-bp DNA at the indicated nanopore diameters ($V = 300$ mV, $T = 21.0 \pm 0.1$°C). Two salient features emerge upon decreasing the pore size: 1), a decrease in I_B (from 0.9 to 0.5); and 2), a drastic increase in t_D of nearly two orders of magnitude.

General properties of the dwell-time and blocked-ion-current distributions

In Fig. 3, we display semilog scatter plots of I_B versus t_D for 8000-bp DNA using 8-nm and 4-nm pores (*blue* and *red markers*, $\langle i_o \rangle_{300\,mV} = 10.0$ and 2.5 nA, respectively). Three main features are apparent. 1), In the 8-nm pore, one-tenth of the open-pore current is blocked by the DNA ($I_B = 0.89 \pm 0.07$), whereas in 4-nm pores, more than half of the open-pore current is blocked, i.e., $I_B = 0.48 \pm 0.05$. 2), Similar to results from previous studies using large pores, events in the 8-nm pore exhibit a substantial fraction of bilevel events, attributed to partially folded DNA entering the pore (14,16). In contrast, we find that events with 4-nm pores are exclusively on a single level, residing in one of two I_B populations, as discussed later. 3), We observe a shift in t_D of nearly two orders of magnitude when the nanopore size is decreased from 8 nm to 4 nm. Although a quantitative analysis of the dwell-time dynamics is provided later, we note that if the translocation time were to simply scale with frictional drag in the pore ($\sim \eta a/(d-a)$, where d is the pore diameter and $a = 2.2$ nm is the hydrodynamic diameter of dsDNA) (17), one would expect a mere threefold increase in translocation times. Thus, the striking difference in t_D qualitatively suggests a nontrivial, powerful dependence of pore size on the translocation dynamics, which we investigate in this article.

In Fig. 4, we present a summary of 2744 events collected for 6000-bp DNA using a 4-nm pore. A 2D scatter plot of I_B versus t_D (Fig. 4 *a*) shows a broad distribution of I_B values (0.4–0.8) and dwell times (20 μs to 100 ms). Moreover, we note that t_D values are not randomly distributed, but rather correlate with the I_B level: on average, shorter events block the pore less than long events. This trend, clearly observed over a time range of 50–500 μs, occurs well within the temporal resolution of our system ($\sim$12 μs, see Fig. S2). To quantitatively correlate the event duration with the current blockage level, we present in Fig. 4 *b* an I_B distribution for all events in the scatter plot. This distribution unambiguously shows two peaks and is well approximated using a double-Gaussian function. The appearance of two I_B peaks is a typical feature of our nanopore experiments, for all examined DNA lengths and temperatures. From the double-Gaussian fit parameters, we split the event populations into low-level (peak at I_{BL}, *green*) and high-level (peak at I_{BH}, *red*) blockades, where the low-level blockades correspond to greater current blockage by the DNA and vice versa. To probe the

TABLE 1 Glossary of symbols

t_D	Event dwell-time
t_P	Most probable translocation time
δt	Time delay between two successive events
t_0	Collision timescale
t_1	Short translocation timescale
t_2	Long translocation timescale
l	DNA length
N	Number of DNA nucleotides or basepairs
$\langle i_o \rangle$	Open-pore current level
$\langle i_b \rangle$	Blocked-pore current level
I_B	Fractional blocked current
$1 - I_B$	Normalized event amplitude
I_{BL}	Low-level current blockade
I_{BH}	High-level current blockade

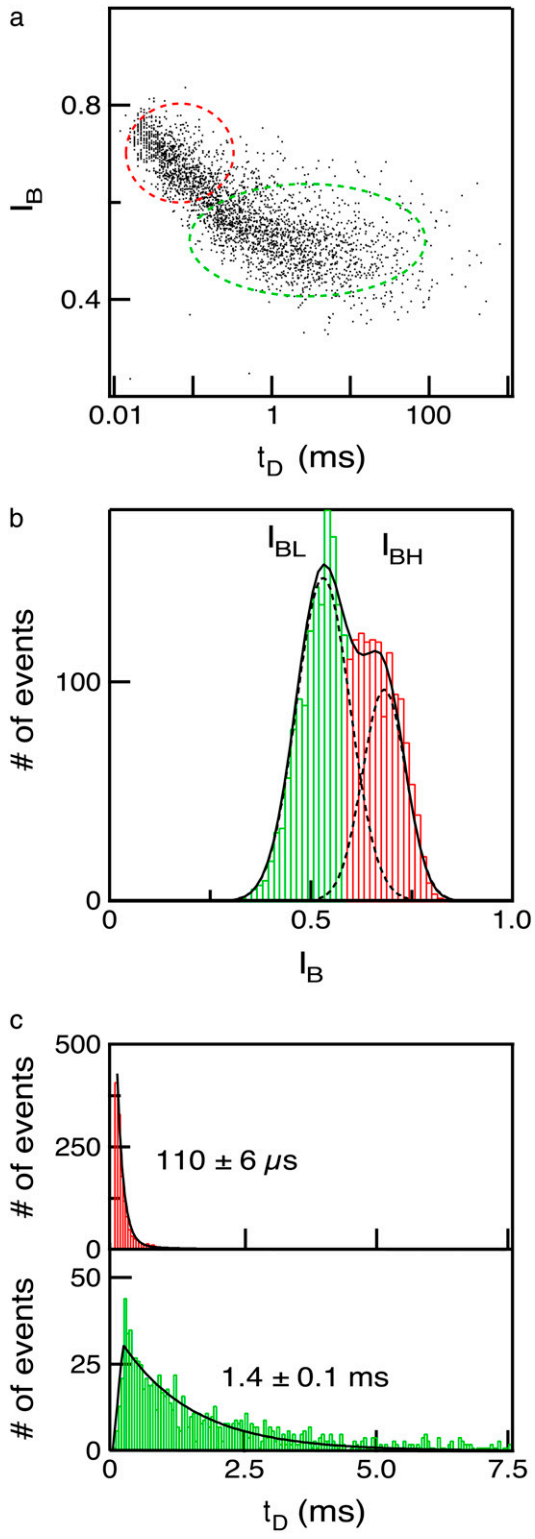

FIGURE 4 Translocation of a 6000-bp DNA fragment using a 4-nm pore (300 mV, 21°C, $n = 2744$ events). (*a*) A 2D scatter plot of I_B versus t_D for all the events, highlighting two distinct populations (*red* and *green ovals*). (*b*) I_B histogram of all the events, revealing two normal distributions, I_{BH} (*red*) and I_{BL} (*green*). (*c*) Histograms of the segregated events based on their respective I_B population, yielding distinct dwell-time distributions for events in the I_{BH} (*upper*) and I_{BL} (*lower*) populations (*solid lines* are fits to the distributions; see text).

dwell-time characteristics of a population, we chose a cutoff that excludes >99% of events in the other population: e.g., a pure I_{BL} population is obtained with a cutoff at $I_{BH} - 2\sigma_H$, where σ_H is the std of the I_{BH} Gaussian.

Upon segregation of the events by their respective I_B populations, we find that the corresponding dwell-time distributions for the two populations are markedly different: The I_{BH} population, which consists of nearly half the events, exclusively contains short t_D values, and the distribution can be well approximated by an exponential function with decay constant $t_0 = 110 \pm 6$ μs (Fig. 4 *c*, *upper*). In contrast, dwell times for the I_{BL} population are much longer. We find that the t_D distribution can be approximated by a sharply increasing function for $t_D < t_P$, and a broad biexponential tail for $t_D > t_P$, with time constants $t_1 = 1.4 \pm 0.1$ ms and $t_2 = 8.0 \pm 0.9$ ms, where $t_P \sim 200 \pm 12$ μs denotes the peak of the distribution (Fig. 4 *c*, *lower*). Since the vast majority of I_{BL} events are spread over the broad tail of the distribution (i.e., $t_1 \gg t_P$), it follows that the average dwell time is primarily determined by a weighted sum of t_1 and t_2 (i.e., not by events with $t_D < t_P$). As discussed in detail below, the relative frequency of the long t_2 events gradually increases with DNA length, becoming the dominant population for DNA longer than several thousand basepairs (in Fig. 3, for example, the broad dwell-time distribution for 8000-bp DNA using the 4-nm pore is comprised of >90% t_2 events). Small changes in the cutoff values for I_{BL} and I_{BH} had negligible impact on determination of the timescales. As demonstrated in the next section, the two I_B levels correspond to either collisions or full translocations.

Effect of pore size on DNA capture probability, blocked current values, and translocation times

Fig. 5 shows characteristic I_B histograms for three pores with $d = 3.1$ nm, 4.0 nm, and 4.6 nm (Fig. 5, *upper*, *middle*, and *lower*, respectively), measured using a 400-bp DNA fragment (300 mV, 21.0°C). As explained above, double-Gaussian fits are used to determine I_{BH} and I_{BL} values, as well as the relative fraction of events in each population, using: $F_L = \left(1+(a_H/a_L)\sqrt{(w_H/w_L)}\right)^{-1}$, where a_H and a_L are the high and low amplitudes, respectively, and w_H and w_L are the high and low widths respectively. The dashed lines display the individual normal distributions for I_{BH} and I_{BL}, as determined from the fits. We find that F_L increases from 0.36 ± 0.03 to 0.83 ± 0.01 as the pore diameter increases from 3.1 to 4.6 nm. This trend is schematically illustrated in green for bins predominantly belonging to the I_{BL} population and in red for those belonging predominantly to the I_{BH} population. We also note that both I_{BH} and I_{BL} gradually increase with the nanopore size.

Additional experiments, using 25 different nanopores (2.7–5 nm) and performed under the same conditions, are shown in Fig. 6. The values of I_{BH} and I_{BL} follow a clearly increasing trend with d. A purely geometrical estimation of

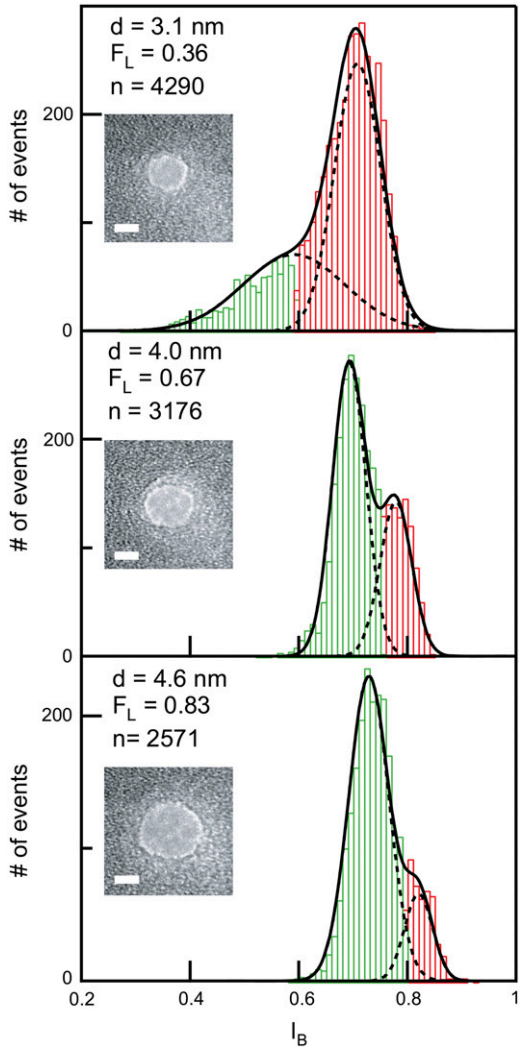

FIGURE 5 I_B histograms for 400-bp DNA at three different nanopore diameters (d). (*Insets*) Transmission electron microscope images of the nanopores (scale bars, 2 nm). The current histograms clearly show two normal populations, described by a sum of two Gaussian functions (*solid black curves*). Each Gaussian function (*dashed lines*) is used to estimate mean I_{BH} and I_{BL} values, as well as the low current fraction, F_L, as defined in the text. Red and green colors are used to highlight the shift in relative populations as a function of d (n denotes the number of events).

the blocked ion current is given by the ratio of the hydrodynamic cross section of B-form dsDNA (a =2.2 nm) to the pore diameter:

$$I_B(d) = 1 - \left(\frac{a}{d}\right)^2. \quad (1)$$

It is remarkable that Eq. 1 (Fig. 6, *dashed line*), which does not involve any scaling factors or fitting parameters, coincides extremely well with measured I_{BL} values, at the same time clearly deviating from the trend of I_{BH} values. Referring back to Fig. 4, we recall that events associated with the I_{BH} population have an extremely short t_D distribution, in contrast to the much broader distribution observed in events of the I_{BL}

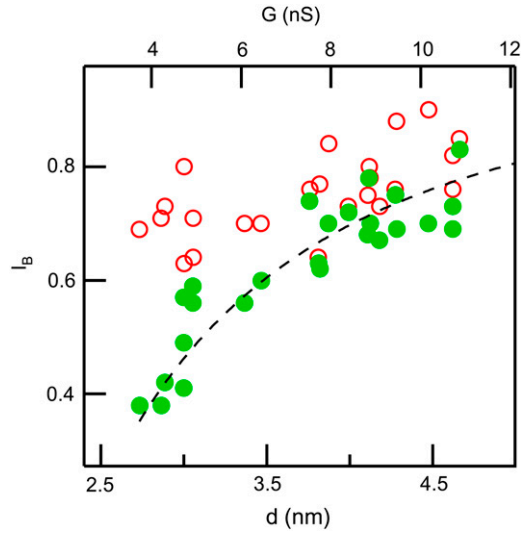

FIGURE 6 I_{BL} (*green*) and I_{BH} (*red*) values for a series of 25 nanopores with different diameters in the range 2.7–4.6 nm, measured using a 400-bp fragment (each I_B pair is based on a histogram of >1500 events, as in Fig. 4). The dashed line is the theoretical I_B^* curve based on Eq. 1, with $a = 2.2$ nm, showing excellent agreement with I_{BL} and clearly deviating from I_{BH}.

population. In the last Results section, we show that characteristic timescales associated with I_{BL} strongly depend on DNA length, whereas timescales associated with I_{BH} exhibit weak length dependence.

The above findings lead us to postulate that events in population I_{BH} correspond to unsuccessful threading attempts (collisions), whereas events in population I_{BL} represent DNA translocations, as supported by 1), the excellent agreement of I_{BL} with Eq. 1, and clear deviation of I_{BH} values from it, 2), the shift in F_L as a function of nanopore size (i.e., more collisions for decreasing nanopore size); 3), the superlinear dependence of DNA length on t_D values for events in the I_{BL} population, and the weak dependence of length on t_D values in the I_{BH} population (see last Results section). Our hypothesis is in accordance with previous investigations of ssDNA translocation through α-HL, which concluded that short (~10-μs) and shallow events (t_0) are random collisions with the pore entrance, whereas longer events (t_1 and t_2) are translocations (7,9,10,26).

Recalling Fig. 3, the vast difference in dwell times between 8-nm pores and 4-nm pores implies that nanopore size plays a crucial role on the dynamics. We expect that as d approaches the diameter of the DNA cross section, small variations in size would strongly affect the extent of DNA/nanopore interactions, but would have negligible effects on the biopolymer configurational energy outside the pore, or on the collision timescale, t_0. Finer insight into the size dependence is given in Fig. 7 *a*, which shows t_1 and t_0 as a function of d, measured using a 400-bp fragment. We observe a striking increase in t_1, by a factor of ~13, when d is reduced from 5.0 to 2.7 nm, well above that expected due to drag inside the pore (a factor of 5.3). Meanwhile, d has marginal influence

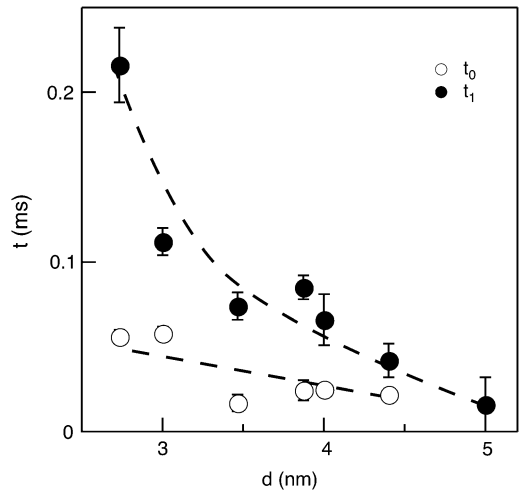

FIGURE 7 Plots of the collision timescale (t_0, *open circles*) and the translocation timescale (t_1, *solid circles*) for 400-bp DNA as a function of nanopore diameters (d) in the range 2.7–5 nm. The lines are guides to the eye.

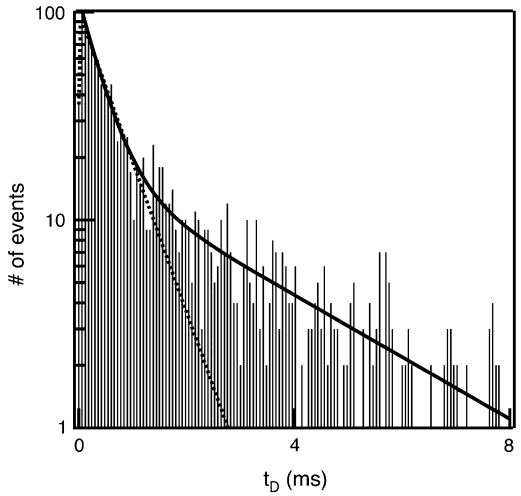

FIGURE 8 Representative dwell-time histogram (1755 events taken from I_{BL} population) for a 2000-bp DNA fragment (4-nm pore, 300 mV, 21°C). A monoexponential fit to the tail of the first-passage time distribution (*dashed line*) yielded poor fits ($\chi^2 > 3$), whereas a double-exponential tail fit (*solid line*) yields excellent agreement with the data, as indicated by a reduced χ^2 value of 1.05. Similar distributions of other representative DNA lengths are shown in Fig. S4 (Data S1).

on t_0, supporting our assignment of t_0 to the collision timescale, and t_1 to the timescale of full DNA translocations. We note that t_2 shows pore-size dependence similar to that of t_1 (not shown); however, the t_2 population is a minority for 400-bp DNA, and extracted t_2 values are associated with large uncertainty.

Dependence of the translocation dynamics on DNA length, blocked current level, voltage, and temperature

We now shift our attention to the dwell-time distributions of events in population I_{BL} as a function of DNA length, ranging from 150 to 20,000 bp (300 mV, 21.0°C). We chose to concentrate on 4-nm pores for this study, because the majority of events for these pores are in the I_{BL} population, and folding is not expected to occur. We extracted characteristic timescales from the dwell-time distributions for a representative set of DNA lengths. A typical distribution for $N = 2000$ bp is shown in Fig. 8 (see Fig. S4 for distributions of other DNA lengths). For comparison, monoexponential (*dashed line*) and double-exponential (*solid line*) fits are overlaid on the distribution. It is evident that the monoexponential functions poorly fit our data, reflected in poor reduced χ^2 values ($\chi^2 > 3$ for all DNA lengths above 400 bp), whereas double-exponential fits yield reduced χ^2 values in the range $\sim 1.0 \pm 0.2$ for all datasets (for each distribution, optimum bin size was chosen to determine both timescales simultaneously). Using models involving three or more exponentials did not improve the goodness of the fits. Although our approach to fit the data is partly empirical, we point out that the tails of translocation distributions are well approximated by exponentially decaying functions. The overlap of two broad populations and a collision timescale with small solid-state pores complicates the determination of exact t_p values, whereas extracted decay timescales are highly robust. We note that with the exception of the shortest DNA (150 bp), translocation timescales t_1 and t_2 were well-resolved from corresponding collision timescales (t_0).

Fig. 9 *a* shows a log-log plot of the three timescales as a function of DNA length. Error bars were determined from the reduced χ^2 analysis in each fit, considering the statistical error of each bin in the dwell-time histogram. As previously noted, t_0 exhibits extremely weak length dependence (*dashed line*). Since the timescales for molecular collisions are governed by DNA diffusion, we can expect a weak length scaling of $t_0(l) \approx l/\ln(l)$, as our data indicates. In contrast, the translocation timescales t_1 and t_2 exhibit a strong dependence on N, displaying a soft transition between two power laws: $t_1 \approx N^{\alpha_1}$, where $\alpha_1 = 1.40 \pm 0.05$, and $t_2 \approx N^{\alpha_2}$, where $\alpha_2 = 2.28 \pm 0.05$ (Fig. 9 *a*, *solid lines*). By defining the relative fraction of long to short events as $D_{t2} = a_2 t_2/(a_1 t_1 + a_2 t_2)$, where a_1 and a_2 are the amplitudes of the double-exponential fits, we find that a transition from a t_1-dominated regime to a t_2-dominated regime occurs near 3500 bp (see Fig. 9 *b*). For each DNA length, the dominant timescale (representing >50% of events) is displayed with a solid marker. Apart from the gradual shift to t_2 timescales, a clear deviation in our extracted t_2 timescales for 400-bp and 1200-bp DNA molecules is observed, which may be a result of error stemming from the low fractions of t_2 events for these DNA lengths.

Fig. 10 displays the dependence of I_{BL} on the DNA length, using 4-nm pores. If one relates I_{BL} solely to the geometric

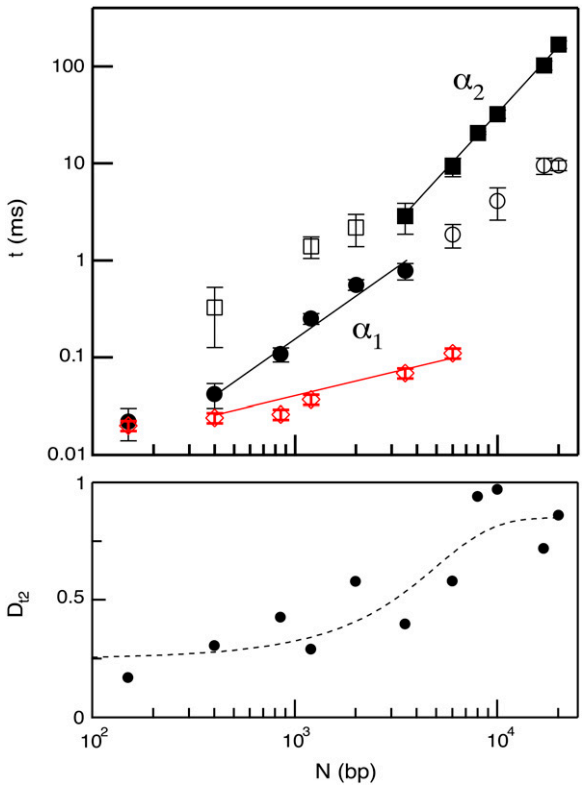

FIGURE 9 (*a*) Log-log plot of DNA translocation timescales as a function of DNA length (N) measured using a 4-nm pore: t_0 (*open diamonds*) attributed to collisions with the pore, t_1 (*circles*) attributed to translocations, which follows a power law with $\alpha_1 = 1.40$, and t_2 (*squares*) attributed to long translocation events, which exhibit a power law with $\alpha_2 = 2.28$. Open markers designate the minor timescale in the population (<50% of events), whereas solid markers represent the dominant timescale. (*b*) Semilog plot of D_{t2}, the fraction of events in the t_2 population (see text), as a function of N. The plot shows a gradual transition from t_1-dominated distributions to t_2-dominated distributions occurring at $N \sim 3500$ bp.

blockage imposed by the DNA (a good approximation under high salt conditions, see Fig. 6), I_{BL} is expected to be independent of N. This is supported by our data: for $150 \leq N \leq 2000$ bp, we find that $I_{BL} = 0.65 \pm 0.05$, close to the expected value of $1 - (2.2/4)^2$, or 0.70. However, for molecules >1200 bp, we observe a regular decrease in I_{BL} with increasing N, which has not been previously observed (similar behavior is observed for the dependence of I_{BH} on N, not shown for clarity). This surprising decrease in I_{BL} for long DNA molecules suggests that a greater fraction of ions is displaced from the pore and its vicinity during translocation.

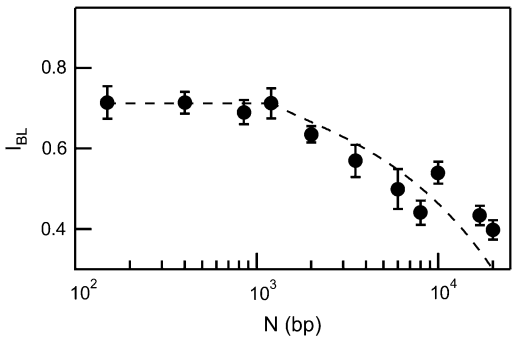

FIGURE 10 Semilog plot of the dependence of the blocked current, I_{BL}, on N, displaying a transition from N-independent to N-dependent regimes at $N > 1200$ bp. The line for $N > 1200$ bp is a power law fit with an exponent of 0.49 ± 0.10.

The observed dependence of the translocation times on DNA length suggests that DNA/pore interactions govern the translocation process. As predicted by recent studies, in the limit of strong interactions we expect nonlinear dependence of translocation times on the applied voltage (22). In Fig. 11, we display a set of measurements of t_1 values for a 400-bp fragment versus applied voltage. As seen in the figure, translocation times strongly decrease with increasing voltage and can be well approximated by an exponential function (*dashed line*). This behavior is expected if DNA/pore interactions are biased by the applied field.

Finally, we investigated the role of temperature on the translocation dynamics. Fig. 12 displays a semilog plot of t_1 (*a*) and t_2 (*b*) for selected DNA lengths as a function of $1/T$. A simplified Arrhenius model for the temperature dependence ($t_T = Ae^{\Delta G/k_B T}$) yields similar effective energy barriers for all DNA lengths, $\Delta G \sim 12.0 \pm 0.5\ k_B T$ (or 7.1 ± 0.3 kcal/mol) for t_1. The invariance of ΔG with N affirms our hypothesis that interactions within the pore dominate the dynamics, since such interactions should not be length-dependent. In contrast, t_2 displays increasing ΔG values for increasing N, with $\Delta G = 18 \pm 1, 25.5 \pm 1, 48 \pm 4$, and $45 \pm 2\ k_B T$ for 1200, 3500, 8000, and 20,000 bp, respectively. This can be rationalized by considering the extent of interactions of the translocating DNA coil with the membrane, which is expected to show length dependence. It should be noted that the slowing down observed with reduced temperature in both t_1 and t_2 cannot be attributed to

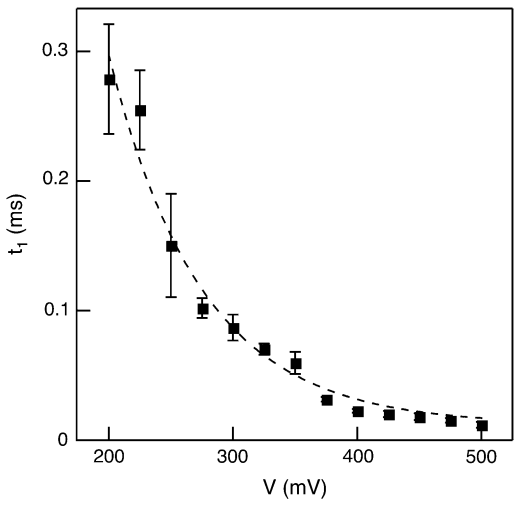

FIGURE 11 Voltage dependence on the translocation dynamics measured for a 400-bp DNA fragment (experiments carried out with a 3.5-nm pore at 21°C). The dashed line is an exponential fit to the data.

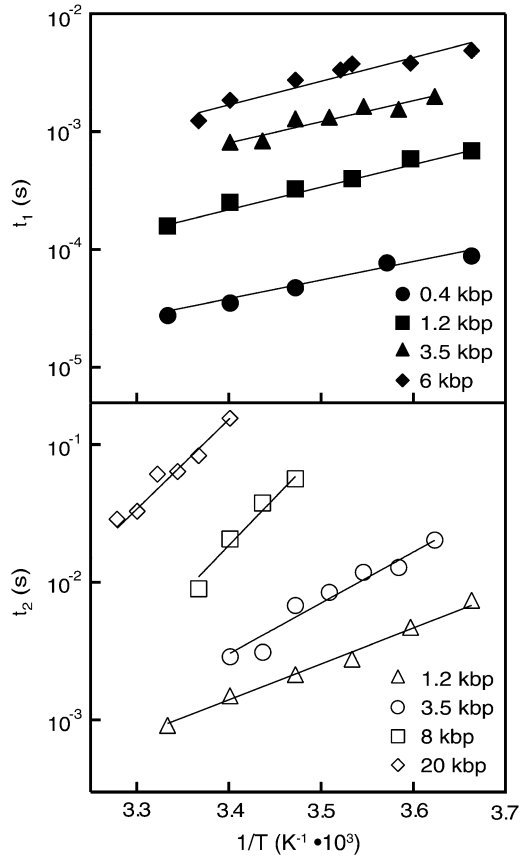

FIGURE 12 Temperature dependence on the translocation dynamics: semilog plot of t_1 (*upper*) and t_2 (*lower*) values for 4-nm pores at the indicated DNA lengths as a function of $1/T$. The lines are Arrhenius fits to the data, with slopes corresponding to energy barriers of $\sim 12.0 \pm 0.5\ k_BT$ for t_1 and 18–48 k_BT for t_2 (see text).

increased fluid viscosity: cooling the electrolyte from 30°C to 0°C results in slowing down by a factor of ~7, whereas in this range of temperatures, viscosity merely increases by ~2.7.

DISCUSSION

Our understanding of the factors governing voltage-driven DNA translocation through solid-state nanopores is to date still lagging. In this article, we systematically analyzed the translocation dynamics as a function of nanopore size, DNA length, voltage, and temperature, in a range where DNA can only enter the nanopore in an unfolded (single-file) configuration. Our main findings can be summarized as follows: first, subtle decreases of the nanopore size result in decreased threading probabilities, markedly larger t_1 values, and marginal impact on the collision timescale t_0. These results, as well as the striking correlation between timescales and current blockage (Fig. 4) and the agreement between the expected I_B based on nanopore size and the measured I_{BL}, confirm that low-level, deep blocking events (i.e., events in I_{BL}) correspond to translocations, whereas shallow events are due to fast collisions. We show here that the translocation time histograms bear resemblance to translocation distributions obtained for ssDNA through α-HL, with two major distinctions: 1), distributions for solid-state nanopores exhibit much broader decays; and 2), monoexponential functions fail to fit the distribution tails, whereas double-exponential functions (with timescales t_1 and t_2) yield excellent fits.

For short dsDNA molecules, where the t_1 timescale is dominant, we note first that the appearance of broad t_D distributions (where $t_1 \gg t_P$) distinguishes the solid-state nanopore system from the ssDNA/α-HL case, where t_D distributions are relatively narrow. In addition, in contrast to the linear dependence of translocation times on DNA length (l) reported for α-HL (27), we find a power-law dependence of $t_1 \approx l^{1.40}$, similar to findings of recent experimental (17,18) and theoretical (28) studies, which reveal/predict a power law of 1.27–1.34 for dsDNA translocation through 8- to 20-nm pores. In particular, our data correspond well to recent Monte-Carlo simulations by Vocks and co-workers, which have predicted for a polymer performing Rouse dynamics a power law scaling of $1+2\nu/1+\nu = 1.37$, where $\nu = 0.59$ is the Flory exponent of the polymer (29).

The order of magnitude increase in measured translocation times with decreasing pore diameter implies that interactions (or drag) inside the pore are the predominant factors governing translocation dynamics. Our voltage and temperature studies suggest that DNA/pore interactions are the main factor governing translocation: for the same pore size, we find an exponential dependence of voltage on mean translocation times, as well as steep Arrhenius temperature dependence on both t_1 and t_2 timescales, much larger than the expected slowing down due to viscosity. These findings isolate DNA/pore interactions as the prevailing mechanism controlling translocation dynamics in small pores.

What, then, is the nature of the DNA/nanopore interactions? A process involving a single, strong binding event (per translocation) may look plausible at first, suggesting Arrhenius-like kinetics. However, a single binding-unbinding mechanism is highly unlikely, as it would be incompatible with the regularity in translocation time dependence on l. On the other hand, the observed dynamics is compatible with a process involving a series of many thermally activated jumps over small energy barriers (possibly each $\sim 12\ k_BT$). In this case, translocation times are expected to scale linearly with the number of energy jumps, thus growing linearly with l. A detailed model for this process is beyond the scope of the current manuscript. We note, however, that in developing a model, one has to take into account the fact that any energy barrier is highly biased by the strong electrical force, which under the conditions employed in our experiment amounts to at least 70 pN, or $\sim 18\ k_BT/\text{nm}$, assuming a Manning screening factor of ~50% inside solid-state nanopores (30).

For long DNA biopolymers, we observe the appearance of a much longer timescale t_2, which has a steeper power law, $t_2 \approx l^{2.28}$. Although the source of this timescale is a subject

for further study, we propose that it is related to additional interactions between external parts of the DNA (i.e., not the DNA region in the nanopore) and the SiN membrane. This is supported by the increasing fraction of t_2-timescale events with increasing DNA length. Although short polymers (several Kuhn lengths) are less likely to interact with the membrane, our observation of a minor t_2 population for short DNA molecules suggests a more complex translocation mode with small pores (e.g., DNA loop interacting with the pore mouth), with the probability increasing with DNA length. Indeed, longer DNA molecules can form more and more interaction sites with the membrane, leading to a prominent t_2 timescale. We note that average translocation times obtained using 4-nm pores are still shorter than the self-relaxation time for dsDNA, as approximated by Rouse or Zimm dynamics (31), implying that the ''frozen'' polymer configuration at the initial moment of threading will determine the translocation dynamics. This may explain the mixture of t_1 and t_2 events with our pores, corresponding to biopolymers that interact only inside the pore and those which also interact with the membrane, respectively.

A striking observation is that I_{BL} values are constant for DNA molecules up to 2000 bp, whereas they decrease for longer molecules. Although there are several possible interpretations for this observation, the external DNA coil above the pore mouth may provide additional resistance to ion flow, further decreasing I_B from its expected geometrical contribution inside the pore. To check our hypothesis, we crudely estimate the increase in the access resistance to the pore by assuming that the long DNA coil forms a sphere of radius R_g and resistivity ρ_{coil}, slightly higher than the bulk resistivity. Since the change in current due to the presence of this sphere near the pore opening is proportional to $\rho_{coil}R_g^3$ and inversely proportional to its area (access resistance), $\Delta I_{BL} \approx \rho_{coil}R_g^3/R_g^2 \approx R_g$. Ignoring all prefactors and using $R_g \approx N^{\nu}$ to estimate the polymer's radius of gyration, it follows that the decrease in I_{BL} for long DNA will scale as $\sim N^{\nu}$. Although this estimation is clearly a crude one, fitting our data in Fig. 10 to a power law yields an exponent of 0.49 ± 0.10 for $N > 2000$ bp (*dashed line*), in qualitative agreement with our rudimentary prediction.

In summary, the focus of our study is the dynamics of dsDNA translocation through solid-state nanopores as a function of their size, temperature, voltage, and DNA length. High-bandwidth measurements have allowed us to resolve short collisions from full translocations, which clearly differ by their blocked-current levels. By decreasing the nanopore size or temperature, we observe an increase in the translocation time of more than an order of magnitude (e.g., ~0.5 ms for 1200 bp), as compared with larger pores, attributable to increased DNA/nanopore interactions. However, smaller pore sizes yield broader, more complex DNA translocation distributions, and a reduced fraction of full translocations to collision. A finer control on the interaction between biological molecules and inorganic pores may be needed to achieve the spatial/temporal resolution required for DNA sequencing and genotyping applications. Manipulating the surface properties of nanopores by coating with inorganic or organic materials (21,32) may achieve this goal. Most important, this study highlights some of the advantages and complexities associated with strong DNA/nanopore interactions in small pores. Although theory and computer simulations have predicted that interaction of polynucleic acids with nanopores can markedly affect the dynamics, we hope our results can stimulate further theoretical and experimental studies, required for a full understanding of the dynamics of DNA translocation through small nanopores.

SUPPLEMENTARY MATERIAL

To view all of the supplemental files associated with this article, visit www.biophysj.org.

We acknowledge valuable input from D. Branton, D. R. Nelson, Y. Rabin, A. Parsegian, and S. Bezrukov. We thank G. V. Soni and A. Squires for reading the manuscript.

We acknowledge support from the Center for Nanoscale Systems at Harvard University, as well as awards from the National Institutes of Health (HG-004128) and the National Science Foundation (PHY-0646637 and NIRT-0403891).

REFERENCES

1. Dekker, C. 2007. Solid-state nanopores. *Nat. Nanotechnol.* 2:209–215.
2. Healy, K. 2007. Nanopore-based single-molecule DNA analysis. *Nanomedicine*. 2:459–481.
3. Wanunu, M., and A. Meller. 2008. Single-molecule analysis of nucleic acids and DNA-protein interactions using nanopores. *In* Single-Molecule Techniques: A Laboratory Manual. P. Selvin, and T. J. Ha, editors. Cold Spring Harbor Laboratory Press, Cold Spring Harbor, NY. 395–420.
4. Hornblower, B., A. Coombs, R. D. Whitaker, A. Kolomeisky, S. J. Picone, A. Meller, and M. Akeson. 2007. Single-molecule analysis of DNA-protein complexes using nanopores. *Nat. Methods*. 4:315–317.
5. Zwolak, M., and M. Di Ventra. 2007. Physical approaches to DNA sequencing and detection. *Rev. Mod. Phys.* 80:141–165.
6. Soni, G. V., and A. Meller. 2007. Progress toward ultrafast DNA sequencing using solid-state nanopores. *Clin. Chem.* 53:1996–2001.
7. Kasianowicz, J. J., E. Brandin, D. Branton, and D. W. Deamer. 1996. Characterization of individual polynucleotide molecules using a membrane channel. *Proc. Natl. Acad. Sci. USA*. 93:13770–13773.
8. Akeson, M., D. Branton, J. J. Kasianowicz, E. Brandin, and D. W. Deamer. 1999. Microsecond time-scale discrimination among polycytidylic acid, polyadenylic acid, and polyuridylic acid as homopolymers or as segments within single RNA molecules. *Biophys. J.* 77: 3227–3233.
9. Meller, A., L. Nivon, E. Brandin, J. Golovchenko, and D. Branton. 2000. Rapid nanopore discrimination between single polynucleotide molecules. *Proc. Natl. Acad. Sci. USA*. 97:1079–1084.
10. Meller, A., L. Nivon, and D. Branton. 2001. Voltage-driven DNA translocations through a nanopore. *Phys. Rev. Lett.* 86:3435–3438.
11. Li, J., D. Stein, C. McMullan, D. Branton, M. J. Aziz, and J. A. Golovchenko. 2001. Ion-beam sculpting at nanometre length scales. *Nature*. 412:166–169.

12. Storm, A. J., J. H. Chen, X. S. Ling, H. W. Zandbergen, and C. Dekker. 2003. Fabrication of solid-state nanopores with single-nanometre precision. *Nat. Mater.* 2:537–540.

13. Kim, M. J., M. Wanunu, D. C. Bell, and A. Meller. 2006. Rapid fabrication of uniformly sized nanopores and nanopore arrays for parallel DNA analysis. *Adv. Mater.* 18:3149–3153.

14. Li, J. L., M. Gershow, D. Stein, E. Brandin, and J. A. Golovchenko. 2003. DNA molecules and configurations in a solid-state nanopore microscope. *Nat. Mater.* 2:611–615.

15. Chen, P., J. J. Gu, E. Brandin, Y. R. Kim, Q. Wang, and D. Branton. 2004. Probing single DNA molecule transport using fabricated nanopores. *Nano Lett.* 4:2293–2298.

16. Storm, A. J., J. H. Chen, H. W. Zandbergen, and C. Dekker. 2005. Translocation of double-strand DNA through a silicon oxide nanopore. *Phys. Rev. E Stat. Nonlin. Soft Matter Phys.* 71:051903.

17. Storm, A. J., C. Storm, J. H. Chen, H. Zandbergen, J. F. Joanny, and C. Dekker. 2005. Fast DNA translocation through a solid-state nanopore. *Nano Lett.* 5:1193–1197.

18. Fologea, D., E. Brandin, J. Uplinger, D. Branton, and J. Li. 2007. DNA conformation and base number simultaneously determined in a nanopore. *Electrophoresis.* 28:3186–3192.

19. Heng, Z. B., C. Ho, T. Kim, R. Timp, A. Aksimentiev, Y. V. Grinkova, S. Sligar, K. Schulten, and G. Timp. 2004. Sizing DNA using a nanometer-diameter pore. *Biophys. J.* 87:2905–2911.

20. Fologea, D., J. Uplinger, B. Thomas, D. S. McNabb, and J. Li. 2005. Slowing DNA translocation in solid-state nanopore. *Nano Lett.* 5: 1734–1737.

21. Chen, P., T. Mitsui, D. B. Farmer, J. Golovchenko, R. G. Gordon, and D. Branton. 2004. Atomic layer deposition to fine-tune the surface properties and diameters of fabricated nanopores. *Nano Lett.* 4:1333–1337.

22. Lubensky, D. K., and D. R. Nelson. 1999. Driven polymer translocation through a narrow pore. *Biophys. J.* 77:1824–1838.

23. Aksimentiev, A., Z. B. Heng, G. Timp, and K. Schulten. 2004. Microscopic kinetics of DNA translocation through synthetic nanopores. *Biophys. J.* 87:2086–2097.

24. Yeh, I. C., and G. Hummer. 2004. Nucleic acid transport through carbon nanotube membranes. *Proc. Natl. Acad. Sci. USA.* 101:12177–12182.

25. Meller, A., and D. Branton. 2002. Single molecule measurements of DNA transport through a nanopore. *Electrophoresis.* 23:2583–2591.

26. Bates, M., M. Burns, and A. Meller. 2003. Dynamics of DNA molecules in a membrane channel probed by active control techniques. *Biophys. J.* 84:2366–2372.

27. Meller, A. 2003. Dynamics of polynucleotide transport through nanometre-scale pores. *J. Phys.: Condens. Matter.* 15:R581–R607.

28. Luo, K., T. Ala-Nissila, and S.-C. Ying. 2006. Polymer translocation through a nanopore under an applied extrnal filed. *J. Chem. Phys.* 124: 114704.

29. Vocks, H., D. Panja, G. T. Barkema, and R. C. Ball. 2008. Pore-blockade times for field-driven polymer translocation. *J. Phys.: Condens. Matter.* 20:095224.

30. Keyser, U. F., B. N. Koeleman, S. Van Dorp, D. Krapf, R. M. M. Smeets, S. G. Lemay, N. H. Dekker, and C. Dekker. 2006. Direct force measurements on DNA in a solid-state nanopore. *Nat. Phys.* 2:473–477.

31. Shusterman, R., S. Alon, T. Gavrinyov, and O. Krichevsky. 2004. Monomer dynamics in double- and single-stranded DNA polymers. *Phys. Rev. Lett.* 92:048303.

32. Wanunu, M., and A. Meller. 2007. Chemically modified solid-state nanopores. *Nano Lett.* 7:1580–1585.